A Hybrid Modulation Strategy With Neutral Point Voltage Balance Capability for Electrolytic Capacitorless Vienna Rectifiers

Zhijian Zhang, Guoqiang Zhang, *Senior Member, IEEE*, Gaolin Wang, *Senior Member, IEEE*, Jiarui Wang, Dawei Ding, *Member, IEEE*, and Dianguo Xu, *Fellow, IEEE*

***Abstract*—Electrolytic capacitorless Vienna rectifiers have many advantages, such as longer lifetime and higher power density. However, the reduced dc-link capacitance aggravates the voltage stress due to the neutral point (NP) fluctuation. In this article, a hybrid modulation strategy combining the modulations of redundant vector and compression vector is proposed, which can realize the NP voltage balance for electrolytic capacitorless Vienna rectifiers. On the basis of analyzing the limitation of NP-balance capability of conventional space vector pulsewidth modulation (PWM) strategy in the region of high modulation index, the negative influence of reduced capacitance on the NP fluctuation and the input current harmonics is revealed. To suppress the NP fluctuation, the compression coefficient is introduced to redistribute the duty cycles of voltage vector, which can reduce the negative effect of medium vector on the NP voltage. In addition, the phase voltage error is modeled to reduce the input current harmonics with the appropriate adjustment factor. The implementation of the proposed strategy is realized by the equivalent carrier-based PWM, which can avoid the sector judgment and angle calculation. By using the proposed strategy, the NP voltage balance and the input current harmonics reduction can be realized simultaneously. The effectiveness of the proposed strategy is verified on an electrolytic capacitorless Vienna rectifier platform.**

***Index Terms*—Current harmonics, electrolytic capacitorless, neutral-point (NP) voltage balance, space vector pulsewidth modulation (SVPWM), Vienna rectifier.**

I. Introduction

With the urgent need for high power density and high reliability, three-level Vienna rectifiers have received special attention in recent years. Compared with the conventional three-level neutral-point-clamped (NPC) rectifiers, Vienna rectifiers have the advantages of simple circuit structure, fewer semiconductor devices, low switching loss and no shoot-through problem [1]–[4]. Therefore, Vienna rectifiers are widely used in wind turbine systems, electric vehicle charging systems, and aircraft systems [5]. However, the Vienna rectifiers have the issue of unbalanced neutral point (NP) voltage [6]. To suppress the unbalanced NP voltage, large-volume electrolytic capacitors are usually adopted at the dc link, which decreases the power density and reliability of Vienna rectifiers [7]. There are important practical implications for replacing electrolytic capacitors with small-volume film capacitors. However, the largely reduced value of dc-link film capacitors will aggravate the problem of the unbalanced NP voltage and cause higher voltage stress on capacitors and switching devices [8]. Therefore, the NP voltage balance needs to be further researched for electrolytic capacitorless Vienna rectifiers.

The unbalanced NP voltages of Vienna rectifiers are mainly divided into two types: the dc unbalance and the ac unbalance [9]. The dc unbalance is the constant voltage difference between the upper and lower capacitors. The carrier-based pulsewidth modulation (CBPWM) can reduce the dc unbalance by injecting the dc component into the modulation wave through proportional-integral (PI) controller [10], [11]. The space vector pulsewidth modulation (SVPWM) can reduce the dc unbalance by distributing the duty cycles of redundant vectors [12], [13]. The dc unbalance mainly depends on unbalanced loads, and it is unrelated with the change of the capacitance [12], [14].

The ac unbalance is a time-varying voltage difference, whose main frequency is three-time that of the grid. The amplitude of ac unbalance is related to the load current, the power factor, the modulation index, and the dc-link capacitors [15]–[17]. In the electrolytic capacitorless Vienna rectifiers, the ac unbalance will be aggravated. Both CBPWM and SVPWM strategies have been used to suppress the ac unbalance, although the latter has usually been finally implemented exploiting the equivalence with the former to simplify the algorithm [18], [19]. For the CBPWM-based strategies, the ac unbalance is suppressed by injecting the zero sequence components into the modulation wave. In [20], the optimal zero-sequence components were injected into CBPWM to suppress the ac unbalance of Vienna rectifiers. To simplify the zero sequence injection, a hybrid method combining a dynamic adjustment factor with a voltage deviation control of the split dc-link was proposed [21]. In [22], a generalized design framework for three-phase Vienna

Manuscript received 18 February 2022; revised 24 May 2022; accepted 13 July 2022. Date of publication 19 July 2022; date of current version 6 September 2022. This work was supported in part by the Research Fund for the National Natural Science Foundation of China under Grants 52125701 and 52177034, and in part by the Fundamental Research Funds for the Central Universities under Grants FRFCU5710092020 and FRFCU5710051220. Recommended for publication by Associate Editor D. Dujic. *(Corresponding author: Guoqiang Zhang.)*

The authors are with the School of Electrical Engineering and Automation, Harbin Institute of Technology, Harbin 150001, China (e-mail: 21b906027@stu.hit.edu.cn; zhgq@hit.edu.cn; wgl818@hit.edu.cn; wangjiarui1874755@163.com; dingdawei_hit@foxmail.com; xudiang@hit.edu.cn).

Color versions of one or more figures in this article are available at https://doi.org/10.1109/TPEL.2022.3192438.

Digital Object Identifier 10.1109/TPEL.2022.3192438

rectifiers was proposed to handle the NP voltage balance issue. In [11], a novel zero-sequence component injection modulation method was presented, which cannot only suppress the NP voltage fluctuation, but also mitigate the input current harmonics of Vienna rectifiers. However, when the modulation index is high, the above methods are easy to enter the overmodulation in advance, resulting in the failure to suppress the ac unbalance for electrolytic capacitorless Vienna rectifiers [23]. For the SVPWM-based strategies, the ac unbalance is suppressed by distributing the duty cycles of redundant vectors. In [24], a two-layer PWM scheme based on vector selection was developed, which can achieve input current harmonics elimination, common-mode voltage reduction, and NP voltage balancing simultaneously. To improve the efficiency of the Vienna rectifier, a discontinuous pulsewidth modulation (DPWM) method was proposed to decrease the switching losses. However, the ability of conventional DPWM methods to balance the NP voltage should be enhanced [25], [26]. In [27], a hybrid DPWM method was proposed, which can suppress the zero-crossing distortion and reduce the NP fluctuation. In [17], a new DPWM method using two different offsets was proposed to realize the NP ripple reduction. In [28], a modified DPWM method was presented to suppress the NP fluctuation by using redundant clamping modes. However, the essence of the above methods is to distribute the duty cycles of redundant vectors to regulate the NP voltage balance. When the modulation index is high, the redundant vector cannot completely offset the influence of the medium vector on the NP voltage in one switching period [29]. Therefore, the NP voltage balance for electrolytic capacitorless Vienna rectifiers is difficult to achieve in the whole linear region.

In order to ensure the NP voltage balance, it is necessary to reduce the influence of the medium vector on the NP voltage when the modulation index is high. For the NPC convert, a virtual-space-vector PWM (VSVPWM) was proposed to suppress the NP fluctuation for the whole modulation index [30], [31]. In [7] and [32], a fast-processing modulation strategy was proposed to simplify the VSVPWM. The above methods can reduce the influence of the medium vector based on the virtual-space-vector concept. These methods need to output three states of positive (P), zero (O), and negative (N) to realize zero NP current in one switching period, which is impossible for Vienna rectifiers owing to the force-commutated current. Consequently, the VSVPWM is not suitable for the Vienna rectifier [11]. In [33], a new switching method called the selected vector was proposed. When the modulation index is high, the method selects two large vectors and a redundant vector to synthesize the reference voltage, which can reduce the negative influence of the medium vector on the NP voltage. However, it is always disabled to output two large vectors in one sector for Vienna rectifiers due to the force-commutated current.

This article proposes a hybrid modulation strategy combining the modulations of redundant vector and compression vector for electrolytic capacitorless Vienna rectifiers to solve the issue of unbalanced NP voltage. The NP fluctuation and the input current harmonics of conventional SVPWM at high modulation index are aggravated with largely reduced dc-link film capacitors. By analyzing the comprehensive causes of the limitation of the NP-balance capability of SVPWM, the compression coefficient is introduced. This coefficient can redistribute the duty cycles of Vienna rectifiers, which is used to reduce the negative effect of medium vector on the NP voltage. The implementation of the proposed strategy is realized by the equivalent CBPWM, which can reduce the sector judgment and the angle calculation. To reduce the harmonics of input currents, the phase voltage error is analyzed to select the appropriate adjustment factor. Compared with the conventional SVPWM, the hybrid modulation strategy can realize the NP voltage balance and the input current harmonics reduction simultaneously. The effectiveness of the proposed strategy is verified on the experimental platform.

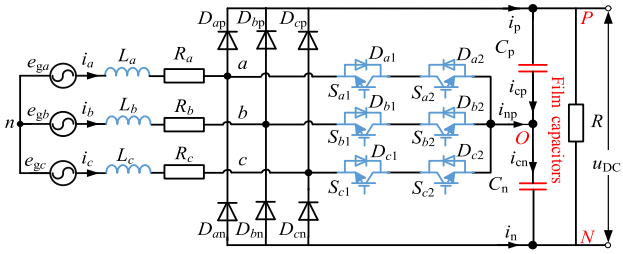

Fig. 1. Topology of electrolytic capacitorless Vienna rectifiers.

II. Analysis of Unbalanced NP Voltage of Electrolytic Capacitorless Vienna Rectifiers

A. NP-Balance Capability of Conventional SVPWM for Electrolytic Capacitorless Vienna Rectifiers

The topology of electrolytic capacitorless Vienna rectifier is shown in Fig. 1, which includes the input filter, the three-phase diode rectifier, the three bidirectional switching units and the film capacitors. In Fig. 1, e_{gx} is the grid voltage, where $x = a$, b, and c. i_x is the input current, u_{xn} is the output voltage between the x phase and midpoint n of grid voltage. R_x and L_x are the x-phase resistance and inductance, respectively. $u_{\rm PO}$ and $u_{\rm ON}$ are the upper and lower DC-link voltages, respectively. $u_{\rm DC}$ is the dc-link voltage. R is the dc-link resistance. The main frequency of NP current is three-time that of the grid [20]. When ignoring other components, the NP current can be expressed as

$$i_{\rm np} = k_{\rm f} m I_m \cos(3\omega t + \varphi) \tag{1}$$

where k_f is the proportional gain of NP fluctuation, m is the modulation index, I_m is the amplitude of the input current, w is the grid frequency, and φ is the initial phase. According to Kirchhoff's law, the voltage difference between the upper and lower capacitors Δu can be expressed as

$$\Delta u = u_{\rm PO} - u_{\rm ON} = -\frac{1}{C}\int_0^t i_{\rm np} dt. \tag{2}$$

According to (2), the cause of unbalanced NP voltage is the presence of the NP current, and Δu is inverse with the capacitance. Therefore, when the volume of dc-link capacitors is small, the unbalanced NP voltage will be aggravated.

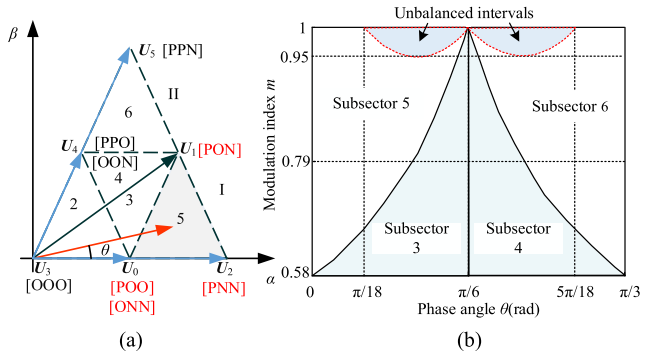

Fig. 2. Distribution of the conventional SVPWM. (a) Vector distribution. (b) Distribution of unbalanced intervals.

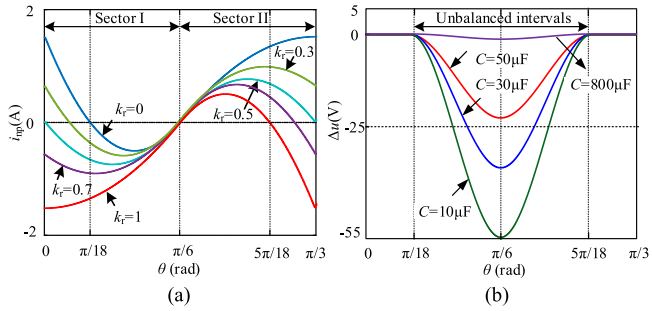

Fig. 3. NP current $i_{\rm np}$ and voltage difference Δu of conventional SVPWM. (a) $i_{\rm np}$ under different k_r. (b) Δu under different capacitances.

To suppress the NP fluctuation, the SVPWM strategy with redundant vector modulation can be adopted. Due to the symmetry, the vector diagram of [0, π/3] is taken as an example to analyze the NP-balance capability of conventional SVPWM, which is shown in Fig. 2(a). The selections of voltage vectors and calculations of duty cycles in other sectors are similar with this vector diagram.

In order to improve dc-link voltage utilization and reduce the voltage stress of the device, the dc-link voltage is set as low as possible, which leads to a relatively high modulation index. When the modulation index is higher, the reference voltage vector mainly passes through subsectors 3–6. According to the volts-second balance rule, the duty cycles of voltage vectors in subsector 5 can be expressed as

$$\begin{cases} d_0 = 2 - m\left(\sqrt{3}\cos\theta + \sin\theta\right) \\ d_1 = 2m\sin\theta \\ d_2 = m\left(\sqrt{3}\cos\theta - \sin\theta\right) - 1 \end{cases} \tag{3}$$

where θ is the phase angle of the reference voltage, d_0, d_1, and d_2 are the duty cycles of small vector $\boldsymbol{U}_0$, medium vector $\boldsymbol{U}_1$ and large vector $\boldsymbol{U}_2$, respectively, and m is the modulation index defined by

$$m = \frac{\sqrt{3}\left|\boldsymbol{U}_{\rm ref}\right|}{u_{\rm DC}} \tag{4}$$

where $|\boldsymbol{U}_{\rm ref}|$ is the modulus of the reference voltage. When the rectifier outputs PON in subsector 5, the b-phase current is connected to O. Therefore, modifying the duty cycle of PON can control b-phase current flowing into the NP. Similarly, the redundant vector ONN can control a-phase current flowing into the NP, and POO has the opposite effect on the NP current. Based on the relationship between the voltage vector and the NP current, $i_{\rm np}$ can be expressed as

$$i_{\rm np} = i_a\left(1 - 2k_{\rm r}\right)d_0 + i_b d_1 \tag{5}$$

where $k_r \in [0, 1]$ corresponds to the distribution factor of the positive redundant vector, such as POO. From the above analysis, the NP fluctuation aggravates under small-value capacitors. Therefore, in order to balance the NP voltage, the NP current should be zero in one switching period. According to (3) and (5), k_r can be calculated as

$$k_{\rm r} = \frac{m\left[-i_a\left(\sqrt{3}\cos\theta + \sin\theta\right) + 2i_b\sin\theta\right] + 2i_a}{2i_a\left[2 - m\left(\sqrt{3}\cos\theta + \sin\theta\right)\right]}. \tag{6}$$

From (6), k_r is related to m and θ. Considering the range of k_r is [0, 1], m needs to meet the following constraints

$$\begin{aligned} &\frac{-2i_a}{\left[-i_a\left(\sqrt{3}\cos\theta+\sin\theta\right)+2i_b\sin\theta\right]} \\ &\le m \le \frac{2i_a}{\left[i_a\left(\sqrt{3}\cos\theta+\sin\theta\right)+2i_b\sin\theta\right]}. \end{aligned} \tag{7}$$

When the Vienna rectifier operates at unity power factor, the input currents can be expressed as

$$\begin{cases} i_a = I_m\cos\left(\theta\right) \\ i_b = I_m\cos\left(\theta - 2\pi/3\right) \\ i_c = I_m\cos\left(\theta + 2\pi/3\right) \end{cases}. \tag{8}$$

According to (7) and (8), the distribution of unbalanced intervals under different m and θ can be obtained, as shown in Fig. 2(b). When m<0.95, the conventional SVPWM can achieve the NP balance, which is unrelated with θ. When m>0.95, some intervals violate the constraint conditions, showing unbalanced intervals. Therefore, when m>0.95, the conventional SVPWM cannot achieve the NP balance in partial intervals, which lead to the NP fluctuation and are proportional to m. Subsectors 3 and 4 can realize the NP balance, regardless of the change of m and θ. When m>0.95, the NP fluctuation mainly occurs in subsectors 5 and 6.

In order to further illustrate the limitation of the NP balance capability of the conventional SVPWM, $i_{\rm np}$ under different k_r based on (3) and (5) is shown in Fig. 3(a). When the reference voltage is located at sector I, the input currents satisfy i_a>0, i_b<0, and i_c<0. When $k_r = 0$, the duty cycle of the redundant vector ONN and POO are the maximum and zero, respectively. According to the influence of voltage vector on the NP current, the NP current reaches the maximum. Similarly, when $k_r = 1$, the NP current reaches the minimum.

It can be seen from Fig. 3(a), when θ is in [0, π/18], the maximum NP current is greater than zero and the minimum NP current is less than zero. There is an appropriate k_r to keep the NP balance. When θ is in [π/18, π/6], the maximum and minimum NP currents are both less than zero. It is impossible to realize the zero NP current by changing k_r. Therefore, to ensure the zero

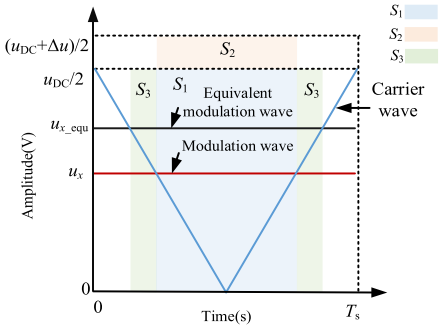

Fig. 4. Impulse diagram with the positive modulation wave.

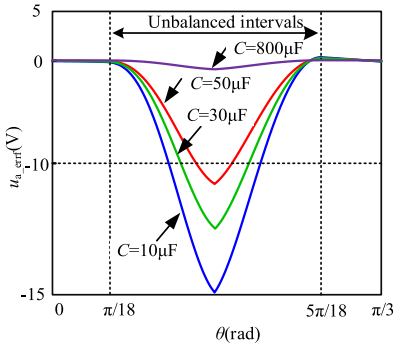

Fig. 5. Phase voltage errors u_{a_errf} with different capacitances.

NP current in one switching period, the NP current should be increased in appropriate intervals.

From (2) and (5), the Δu under different capacitance of conventional SVPWM is obtained, as shown in Fig. 3(b). It can be seen that Δu is not zero in the unbalanced intervals, resulting in the NP fluctuation whose frequency is three-time that of the grid. With the decrease of capacitance, the peak of the NP fluctuation increases significantly. As a result, when m>0.95, the conventional SVPWM cannot realize the NP balance due to the existence of unbalanced intervals. Moreover, due to the largely reduced dc-link film capacitors, the NP fluctuation is further aggravated.

B. Analysis of the NP Fluctuation Influence on Input Currents of Vienna Rectifiers

The NP fluctuation not only increases the voltage stress, but also causes the distortions of input currents. To obtain the effect of the NP fluctuation on the input currents, the impulse equivalency is used. When the modulation wave is positive, the impulse is shown in Fig. 4. When the upper and lower voltages are equal, the impulse of modulated wave u_x corresponds to S_1. When the capacitor voltage is deviated from Δu, the actual impulse is (S_1+S_2). It can be seen that the NP fluctuation leads to the deviation of the impulse of the Vienna rectifier.

To analyze the influence of the NP fluctuation on the modulation wave, the impulse $(S_1 + S_2)$ can be equivalent to the impulse $(S_1 + S_3)$ of NP balance, and the corresponding modulated wave is

$$u_{x\_\mathrm{equ}} = u_x + \frac{\Delta u}{u_{\mathrm{DC}}} u_x \tag{9}$$

where u_x is the x-phase modulation wave with balanced NP voltage, and u_{x_equ} is the equivalent modulation wave with the unbalanced NP voltage.

Similarly, when the modulation wave of the Vienna rectifier is negative, the equivalent modulation wave is

$$u_{x\_\mathrm{equ}} = u_x - \frac{\Delta u}{u_{\mathrm{DC}}} u_x. \tag{10}$$

Based on (9) and (10), the equivalent modulation wave with the unbalanced NP voltage is uniformly written as

$$u_{x\_\mathrm{equ}} = u_x + \frac{\Delta u}{u_{\mathrm{DC}}} |u_x| . \tag{11}$$

Substituting (2) into (11), the modulation wave including the NP fluctuation can be obtained

$$u_{x\_\mathrm{f}} = u_x - \frac{k_{\mathrm{f}} m I_{\mathrm{m}} \left[\sin(3\omega t + \varphi) - \sin\varphi\right]}{3\omega C u_{\mathrm{DC}}} |u_x| . \tag{12}$$

It can be seen that the modulation wave has the error, which is inverse with capacitance. Therefore, the error of modulation wave will further increase with reduced dc-link capacitors.

In order to analyze the influence of the error on the input currents, the relationship between the actual modulation wave u_{x_act} and i_x is

$$i_x = \frac{e_{gx} - u_{xn}}{R_x + sL_x} \tag{13}$$

$$u_{xn} = u_{x\_\mathrm{ref}} + u_{x\_\mathrm{err}} \tag{14}$$

$$u_{x\_\mathrm{err}} = u_{x\_\mathrm{act}} - u_{x\_\mathrm{ref}} - \frac{\sum u_{x\_\mathrm{act}}}{3} \tag{15}$$

where u_{x_ref} is the x-phase sinusoidal modulation wave, and u_{x_err} is the x-phase voltage error. According to (13) and (14), it can be seen that when $u_{x\_\mathrm{err}} = 0$, the harmonics of the input currents are zero with the ideal grid voltage. When $u_{x\_\mathrm{err}} \neq 0$, the harmonics of input currents are the same with those of the phase voltage errors, which are proportional to u_{x_err}. Based on (11) and (15), the a-phase voltage error u_{a_errf} caused by the NP fluctuation can be expressed as

$$u_{a\_\mathrm{errf}} = \frac{\Delta u \left(2|u_a| - |u_b| - |u_c|\right)}{3u_{\mathrm{DC}}}. \tag{16}$$

Combing (2) and (16), phase voltage errors of different capacitance are shown in Fig. 5. It can be seen that there is phase voltage error at unbalanced intervals. Moreover, the phase voltage error will further increase with capacitance decreasing, which will increase the harmonics of input currents.

Therefore, the largely reduced dc-link capacitors aggravate the NP fluctuation and the harmonics of the input currents, and it is important to develop control algorithm to ensure the NP balance.

III. Proposed Hybrid Modulation Strategy for Electrolytic Capacitorless Vienna Rectifiers

In order to ensure the NP voltage balance for electrolytic capacitorless Vienna rectifiers, a hybrid modulation strategy is

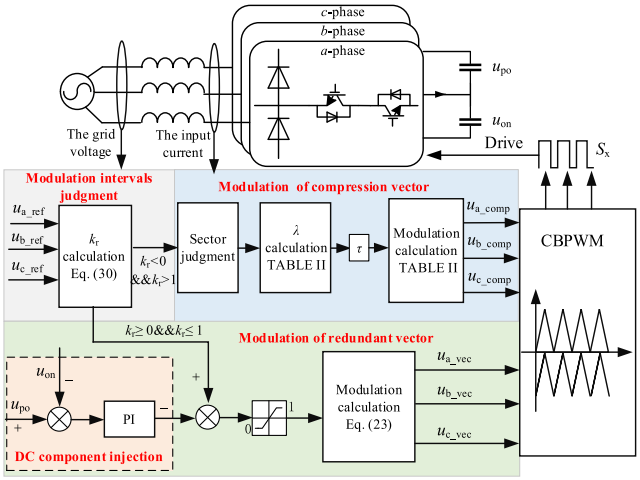

Fig. 6. Block diagram of the proposed strategy.

proposed, which combines the modulations of redundant vector and compression vector. To simplify the proposed strategy, the implementation is realized by CBPWM. The block diagram of the proposed strategy is shown in Fig. 6.

A. Principle of the Proposed Strategy

To realize the NP balance, the compression coefficient λ is introduced, whose range is [0, 1]. The duty cycle of subsector 5 can be written as

$$\begin{cases} d_{0\_\mathrm{comp}} = (1-\lambda)\, d_1 + d_0 \\ d_{1\_\mathrm{comp}} = \lambda d_1 \\ d_{2\_\mathrm{comp}} = d_2 \end{cases} \tag{17}$$

where d_{0_comp}, d_{1_comp}, and d_{2_comp} are the duty cycles of $\boldsymbol{U}_0$, $\boldsymbol{U}_1$ and $\boldsymbol{U}_2$ introduced λ, respectively. According to (3) and (17), the influence of λ on duty cycles can be obtained, as shown in Fig. 7. The duty cycle of each vector is the same as that of the conventional SVPWM when $\lambda = 1$. With the increase of θ, the duty cycle of medium vector increases, while the duty cycles of redundant and large vectors are reduced. Since the NP current of medium vector is uncontrolled, the NP-balance capability of conventional SVPWM is limited. When $\lambda \neq 1$ and $\theta \in [\pi/18, \pi/6]$, the duty cycles of redundant vector and medium vector have changed, which are inverse to λ. When $\lambda = 0$, the duty cycle of medium vector is zero, while the duty cycle of the redundant vector reaches the maximum.

Therefore, the negative influences of the medium vector on the NP current can be reduced with the decrease of λ, which is beneficial to keep NP balance. The NP current with λ can be obtained as

$$i_{\mathrm{np}} = i_a \left[(1-\lambda)\, d_1 + d_0\right](1 - 2k_{\mathrm{r}}) + i_b \lambda d_1. \tag{18}$$

According to (5) and (18), the *a*-phase and *b*-phase currents flowing into the NP are increased and reduced when $\lambda < 1$, respectively. Considering $i_a > 0 > i_b$, the NP current at sector I is increased, which is beneficial to $i_{\mathrm{np}} = 0$. According to (18), both λ and k_r can regulate the NP current. In Fig. 7, λ changes

TABLE I
DISTRIBUTION FACTOR AND COMPRESSION COEFFICIENT OF SECTORS

Sector	Distribution factor k_{r}	Compression coefficient λ
I/III/V	k_{r}=0	$\dfrac{i_{\max}(d_0+d_1)}{d_1(i_{\max}-i_{\mathrm{mid}})}$
II/IV/VI	k_{r}=1	$\dfrac{(d_0+d_1)i_{\min}}{d_1(i_{\min}-i_{\mathrm{mid}})}$

the duty cycles of voltage vectors. Therefore, λ is inverse to the error of synthetic voltage.

In order to select proper k_r and λ, it can get corresponding λ under different k_r and θ, as shown in Fig. 8.

It can be seen that when $k_r > 0.5$, λ exceeds the range of [0, 1], indicating there is no solution. When $k_r \in [0, 0.5]$, λ is inverse to k_{r}. Therefore, it can select $k_r = 0$ to reduce the error of synthetic voltage. This result can be illustrated according to Fig. 3(a). It can be seen that the maximum and minimum NP current is less than zero when $\theta \in [\pi/18, \pi/6]$. In order to reduce the error of synthetic voltage, the maximum current should be increased to zero, which is corresponding to $k_r = 0$. Similarly, the maximum and minimum NP current is greater than zero when $\theta \in [\pi/6, 5\pi/18]$. The minimum current is reduced to zero, which is corresponding to $k_r = 1$.

When k_r is known, λ can be expressed as

$$\lambda = \frac{i_a\,(d_0 + d_1)}{d_1\,(i_a - i_b)}. \tag{19}$$

The values of k_r and λ in different sectors are given in Table I, where $i_{\max}$, i_{mid}, and $i_{\min}$ are maximum, middle, and minimum input currents, respectively.

The introduction of λ can realize the NP balance, but it also causes the error of synthetic voltage. In order to further improve the performance of the Vienna rectifier, the adjustment factor $\tau \in [1, 1/\lambda]$ is introduced. The relationship of τ and λ is

$$\lambda_{\mathrm{adj}} = \tau\lambda \tag{20}$$

where λ_{adj} is the adjusted compression coefficient. According to (2) and (20), the NP fluctuation under different θ is shown in Fig. 9. Compared with SVPWM with $k_r = 0.5$, the NP fluctuation of the proposed strategy is reduced because there is no NP fluctuation in some intervals. When $\tau = 1$, the NP fluctuation is zero, and there is the error of synthetic voltage. When $\tau = 1/\lambda$, it can get $\lambda_{\mathrm{adj}} = 1$ according to (20), and the NP fluctuation reaches the maximum. According to Fig. 7, synthetic voltage has no error currently. Therefore, τ can adjust the NP fluctuation and the error of synthetic voltage.

B. Implementation of Hybrid Modulation Strategy

1) Modulation of Redundant Vector: From the above analysis, the NP balance in partial intervals can be realized by distributing the duty cycles of redundant vectors, such as $[0, \pi/18]$, which is defined as the modulation of redundant vector. In [12], the SVPWM in Vienna rectifier is equivalent to the injection of common-mode components at three-phase

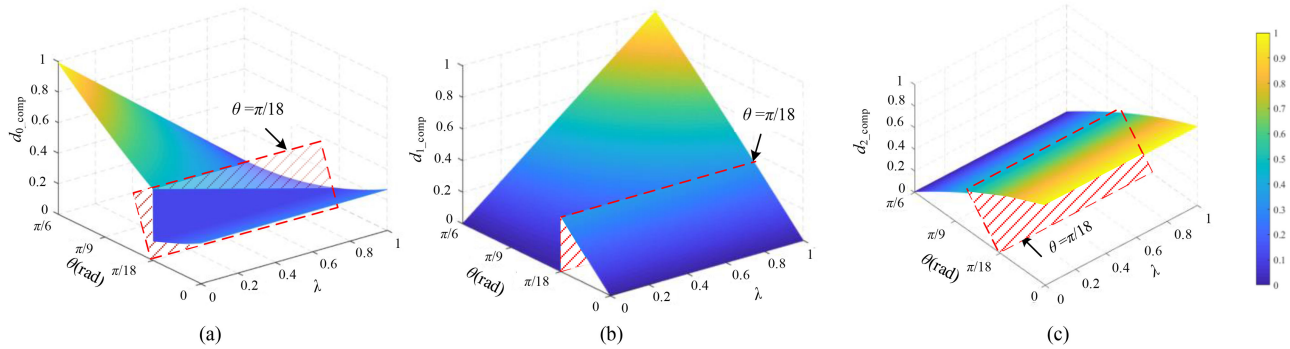

Fig. 7. Influence of λ on duty cycles. (a) Duty cycle of $\boldsymbol{U}_0$. (b) Duty cycle of $\boldsymbol{U}_1$. (c) Duty cycle of $\boldsymbol{U}_2$.

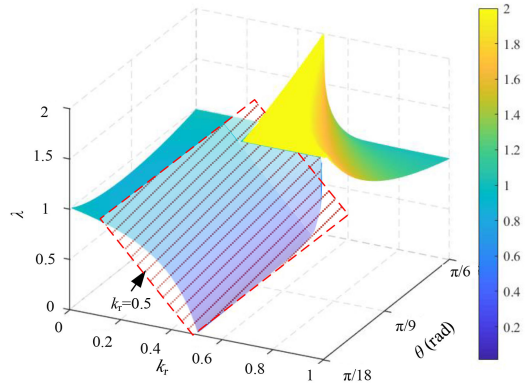

Fig. 8. Corresponding λ under different distribution factors k_{r} and phase angle θ.

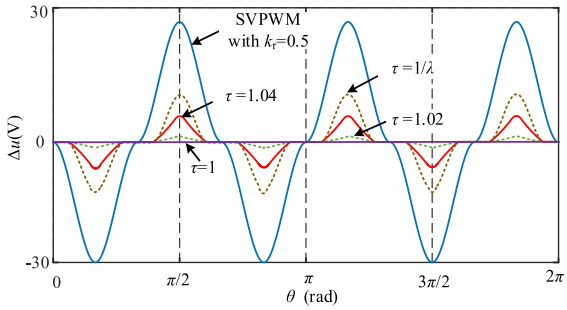

Fig. 9. NP fluctuation under different θ.

sinusoidal modulation waves. With the normalization of u_{x_ref} by $u_{\mathrm{DC}}/2$, the three-phase sinusoidal modulation waves can be expressed as

$$\begin{cases} u_{a\_\mathrm{ref}} = 2/\sqrt{3} m \cos\theta \\ u_{b\_\mathrm{ref}} = 2/\sqrt{3} m \cos\left(\theta - 2\pi/3\right) \\ u_{c\_\mathrm{ref}} = 2/\sqrt{3} m \cos\left(\theta + 2\pi/3\right) \end{cases}. \tag{21}$$

The injected common-mode component is

$$u_{\mathrm{com}} = k_{\mathrm{r}}\left(1 - w_{\max} + w_{\min}\right) - w_{\min} \tag{22}$$

where $w_{\max}$ and $w_{\min}$ are the maximum and minimum values of w_{x}, respectively, and $w_x = \begin{cases} u_{x\_\mathrm{ref}} & u_{x\_\mathrm{ref}} \geq 0 \\ u_{x\_\mathrm{ref}} + 1 & u_{x\_\mathrm{ref}} < 0 \end{cases}$.

The modulation wave of the redundant vector can be expressed as

$$\begin{cases} u_{a\_\mathrm{vec}} = u_{a\_\mathrm{ref}} + u_{\mathrm{com}} \\ u_{b\_\mathrm{vec}} = u_{b\_\mathrm{ref}} + u_{\mathrm{com}} \\ u_{c\_\mathrm{vec}} = u_{c\_\mathrm{ref}} + u_{\mathrm{com}} \end{cases} \tag{23}$$

where u_{a_vec}, u_{b_vec}, and u_{c_vec} are the three-phase modulation waves of the redundant vector, respectively.

Although the proposed strategy can achieve zero NP current in one switching period, the initial potential of the capacitor may be different due to the charging speed and the capacitance volume, which requires balance control. The dc components can be injected into the modulation wave through PI controller to solve the dc unbalance, as shown in Fig. 6.

2) Modulation of Compression Vector: According to Table I, it can be seen that the calculation of λ is related to sectors. For the judgment of I/III/V and II/IV/VI, the sign of the middle current i_{mid} is selected: when $i_{\mathrm{mid}}<0$, the reference voltage is located at sector I/III/V, otherwise it is located at sector II/IV/VI.

To simplify the proposed strategy, the modulation wave with $\lambda = 1$ is obtained firstly. From (23), the modulation wave of subsector 5 with $k_r = 0$ can be expressed as

$$\begin{cases} u_{a\_1} = u_{b\_\mathrm{ref}} - u_{c\_\mathrm{ref}} - 1 \\ u_{b\_1} = u_{b\_\mathrm{ref}} - u_{c\_\mathrm{ref}} - 1 \\ u_{c\_1} = -1 \end{cases} \tag{24}$$

where u_{a_1}, u_{b_1}, and u_{c_1} are the three-phase modulation waves when $\lambda = 1$.

The relationship between the duty cycle and modulation wave is

$$\begin{cases} d_0 = 1 - u_{a\_1} \\ d_1 = 1 + u_{b\_1} \end{cases}. \tag{25}$$

According to (19) and (25), λ can be obtained as follows:

$$\lambda = \frac{\left(2 - u_{a\_1} + u_{b\_1}\right) i_a}{\left(u_{b\_1} + 1\right)\left(i_a - i_b\right)}. \tag{26}$$

Based on CBPWM, the relationship between the duty cycle and modulation wave of redundant vector can be calculated as

$$\begin{cases} u_{a\_\mathrm{comp}} = 1 - \left[\left(1 - \lambda_{\mathrm{adj}}\right) d_1 + d_0\right] \\ u_{b\_\mathrm{comp}} = \lambda_{\mathrm{adj}} d_1 - 1 \\ u_{c\_\mathrm{comp}} = -1 \end{cases} \tag{27}$$

TABLE II
MODULATION WAVES AND COMPRESSION COEFFICIENTS OF DIFFERENT SECTORS

Sectors	Modulation wave with λ=1	Modulation wave with λ_{adj}	Compression coefficient λ
I/III/V	$u_{max\_1}= u_{ref\_max}-u_{ref\_min}-1$ $u_{mid\_1}= u_{ref\_mid}-u_{ref\_min}-1$ $u_{min}= -1$	$u_{max\_comp}=u_{max\_1}+(\lambda_{adj}-1)(u_{mid\_1}+1)$ $u_{mid\_comp} =\lambda_{adj}(u_{mid\_1}+1)-1$ $u_{min\_comp} = -1$	$\frac{(2-u_{max\_1}+u_{mid\_1})i_{max}}{(u_{mid\_1}+1)(i_{max}-i_{mid})}$
II/IV/VI	$u_{max\_1}=1$ $u_{mid\_1}= u_{ref\_mid}- u_{ref\_max}+1$ $u_{min\_1}= u_{ref\_min}- u_{ref\_max}+1$	$u_{max\_comp} =1$ $u_{mid\_comp} =\lambda_{adj}(u_{mid\_1}-1)+1$ $u_{min\_comp} = u_{min\_1}+(\lambda_{adj}-1)(u_{mid\_1}-1)$	$\frac{(2-u_{mid\_1}+u_{min\_1})i_{min}}{(1-u_{mid\_1})(i_{min}-i_{mid})}$

where u_{a_comp}, u_{b_comp}, and u_{c_comp} are the three-phase modulation waves of compression coefficient. Combing (25) and (27), the modulation wave of redundant vector can be expressed as

$$\begin{cases} u_{a\_comp} = u_{a\_1} - (1-\lambda_{adj})(u_{b\_1}+1) \\ u_{b\_comp} = \lambda_{adj}(u_{b\_1}+1) - 1 \\ u_{c\_comp} = -1 \end{cases}. \tag{28}$$

Modulation waves and compression coefficients of different sectors are given in Table II, where u_{max_1}, u_{mid_1}, and u_{min_1} are the maximum, middle and minimum of u_{x_1}, and u_{max_comp}, u_{mid_comp}, and u_{min_comp} are the maximum, middle, and minimum of u_{x_comp}, respectively.

3) Modulation Intervals Judgment: In order to generate the correct modulation wave, the modulations of redundant vector and the compression coefficient need to judge. When $k_r \in [0, 1]$, it belongs to the modulation of redundant vector, otherwise it belongs to the modulation intervals of the compression coefficient. In order to calculate k_r, the NP current in the modulation intervals of redundant vector can be expressed as

$$i_{np} = -u_{a\_vec}|i_a| - u_{b\_vec}|i_b| - u_{c\_vec}|i_c|. \tag{29}$$

When $i_{np} = 0$, k_r can be obtained as

$$k_r = \frac{-\frac{u_{a\_ref}|i_a|+u_{b\_ref}|i_b|+u_{c\_ref}|i_c|}{|i_a|+|i_b|+|i_c|} + w_{min}}{1 - w_{max} + w_{min}}. \tag{30}$$

From the above analysis, it can be seen that the implementation of the proposed strategy can be realized through four operations on the premise of three-phase sinusoidal modulation waves, which can reduce sector judgment and angle calculation.

C. Evaluation of the NP Fluctuation and the Input Current Harmonics of the Proposed Strategy

According to Table II, the a-phase modulation wave of the proposed strategy is

$$\begin{cases} u_{a\_1} - (1-\lambda_{adj})(u_{b\_1}+1) & \theta \in \left[0, \frac{\pi}{6}\right] \& k_r \notin [0,1] \\ 1 & \theta \in \left[\frac{\pi}{6}, \frac{\pi}{3}\right] \& k_r \notin [0,1] \\ \lambda_{adj}(u_{a\_1}-1)+1 & \theta \in \left[\frac{\pi}{3}, \frac{\pi}{2}\right] \& k_r \notin [0,1] \\ \lambda_{adj}(u_{a\_1}+1)-1 & \theta \in \left[\frac{\pi}{2}, \frac{2\pi}{3}\right] \& k_r \notin [0,1] \\ -1 & \theta \in \left[\frac{2\pi}{3}, \frac{5\pi}{6}\right] \& k_r \notin [0,1] \\ u_{a\_1} + (\lambda_{adj}-1)(u_c - 1) & \theta \in \left[\frac{5\pi}{6}, \pi\right] \& k_r \notin [0,1] \\ u_{a\_1} & \theta \in [0,\pi] \& k_r \in [0,1] \end{cases}. \tag{31}$$

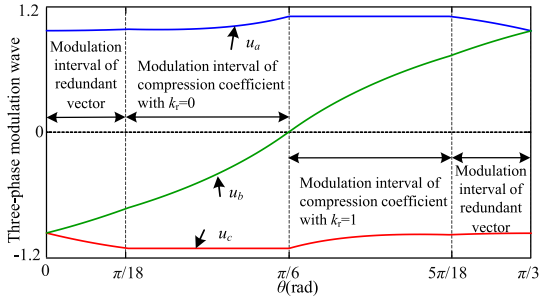

Fig. 10. Three-phase modulation waveforms of the proposed strategy.

According to (31), the three-phase modulation waveform is shown in Fig. 10. It can be seen that the c-phase voltage is clamped to -1 in the modulation intervals of the compression coefficient when $k_r = 0$. The main reason is that the reference voltage vector is synthesized by ONN, PON, and PNN, which is beneficial to reduce the switching losses.

In order to analyze the harmonics of input currents in the modulation intervals of the compression coefficient, the a-phase voltage error u_{a_errp} caused by compression coefficient based on (15) and (31) can be expressed as

$$\begin{cases} \frac{(\lambda_{adj}-1)(u_{b\_1}+1)}{3} & \theta \in \left[0, \frac{\pi}{6}\right] \& k_r \notin [0,1] \\ -\frac{2(\lambda_{adj}-1)(u_{b\_1}-1)}{3} & \theta \in \left[\frac{\pi}{6}, \frac{\pi}{3}\right] \& k_r \notin [0,1] \\ \frac{(\lambda_{adj}-1)(u_a-1)}{3} & \theta \in \left[\frac{\pi}{3}, \frac{\pi}{2}\right] \& k_r \notin [0,1] \\ \frac{(\lambda_{adj}-1)(u_{a\_1}+1)}{3} & \theta \in \left[\frac{\pi}{2}, \frac{2\pi}{3}\right] \& k_r \notin [0,1] \\ -\frac{2(\lambda_{adj}-1)(u_{c\_1}+1)}{3} & \theta \in \left[\frac{2\pi}{3}, \frac{5\pi}{6}\right] \& k_r \notin [0,1] \\ \frac{(\lambda_{adj}-1)(u_{c\_1}-1)}{3} & \theta \in \left[\frac{5\pi}{6}, \pi\right] \& k_r \notin [0,1] \end{cases}. \tag{32}$$

It can be seen that u_{a_errp} is inverse to λ_{adj} and turns to zero when $\lambda_{adj} = 1$. Therefore, it can select different τ to adjust the harmonics of input currents. In Fig. 9, it can be seen that there is NP fluctuation when $\tau \neq 1$. Therefore, the phase voltage error of the proposed strategy is composed of the NP fluctuation and $\lambda_{adj} \neq 1$, and its root mean square (RMS) is

$$\sum u_{err} = \sqrt{\frac{1}{2\pi}\int_0^{2\pi} (u_{a\_errf})^2 d\theta} + \sqrt{\frac{1}{\pi}\int_0^{\pi} (u_{a\_errp})^2 d\theta}. \tag{33}$$

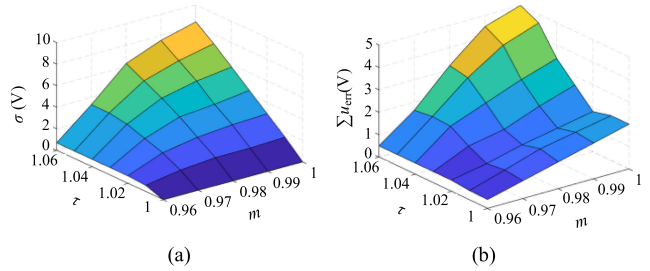

Fig. 11. Variations of σ and $\Sigma u_{\rm err}$ under different adjustment factors τ and modulation index m. (a) Variation of σ. (b) Variation of $\Sigma u_{\rm err}$.

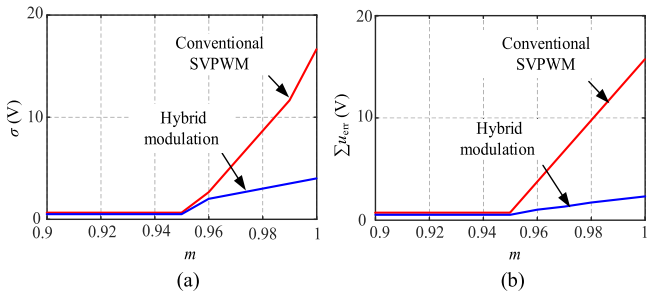

Fig. 12. Comparison results between the conventional SVPWM and the proposed strategy. (a) Comparison results of σ. (b) Comparison results of $\Sigma u_{\rm err}$.

In order to evaluate the NP fluctuation of the proposed strategy, the RMS of NP fluctuation is introduced

$$\sigma = \sqrt{\frac{1}{2\pi}\int_0^{2\pi} (\Delta u)^2 d\theta}. \tag{34}$$

Variations of σ and $\Sigma u_{\rm err}$ under different τ and m are shown in Fig. 11, where $u_{\rm DC} = 120$ V and $C = 10$ μF. According to Fig. 11(a), the NP fluctuation is proportional to m, which is mainly due to the increase of the unbalanced intervals. τ is inverse to the NP fluctuation. Therefore, it can change the NP fluctuation with different τ. According to Fig. 11(b), the harmonics of input currents is proportional to m. When m<0.97, the harmonics of input currents is basically independent with τ. When m>0.97, the harmonics of input currents decreases initially and increases afterward with the increase of τ. Therefore, to reduce the NP fluctuation and harmonics of input currents, $\tau = 1.02$ is selected.

When $\tau = 1.02$, the comparison results between the conventional SVPWM and the proposed strategy are shown in Fig. 12. It can be seen that the proposed strategy can reduce the NP fluctuation and harmonics of input currents, simultaneously.

IV. Experimental Results

The proposed strategy was verified on a Vienna rectifier experimental platform with film capacitors, as shown in Fig. 13. The inverter includes 10-μF film capacitors, the power board, and the control board. The bidirectional switch is constructed by integrating two IPP65R190C7 MOSFETs and it is driven by the UCC21520 driver. The diodes used are SiC C4D08120 A. The whole algorithm is executed on the TMS320F28379D control board. The Chroma61512 is used to provide the ac-power source.

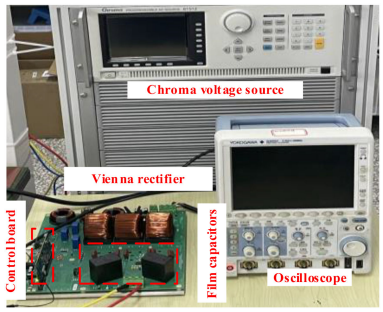

Fig. 13. Experimental platform of Vienna rectifier with film capacitors.

TABLE III
Parameters of Vienna Rectifier

Parameter	Value
Phase voltage	45 V
Grid frequency	50 Hz
Switching frequency	50 kHz
Input inductance	3 mH
Input current	4 A
DC-link capacitance	10 μF
DC-link resistance	29 Ω

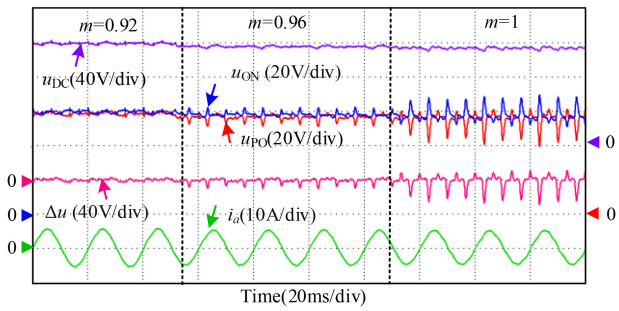

Fig. 14. Experimental results of conventional SVPWM under different m.

Experimental waveforms are acquired by a waveform recorder DLM2054. The parameters of Vienna rectifier are given in Table III.

In order to verify the NP-balance capability of conventional SVPWM, the experimental results under different m are shown in Fig. 14. It can be seen that when $m = 0.92$, the SVPWM can realize the NP balance and there is no NP fluctuation. The maximum RMS of Δu is 1.5 V, which is 1.3% of the dc-link voltage. When $m = 0.96$, there is NP fluctuation, whose frequency is three-time that of the grid and RMS is 2.5%. When $m = 1$, the NP fluctuation is larger due to the increase of the unbalanced intervals. The RMS of Δu is 17 V, which is 15% of the dc-link voltage. Therefore, the conventional SVPWM cannot realize the NP balance for electrolytic capacitorless Vienna rectifiers, and the RMS of Δu is larger with the increase of m. The experimental results are consistent with Section II-A.

Experimental results of different strategies when $m = 0.96$ are shown in Fig. 15. In Fig. 15(a), the NP fluctuation of conventional SVPWM with $k = 0.5$ is the largest, which leads to input current distortions. In Fig. 15(b), modulation of redundant vector can reduce the NP fluctuation, but it cannot realize the

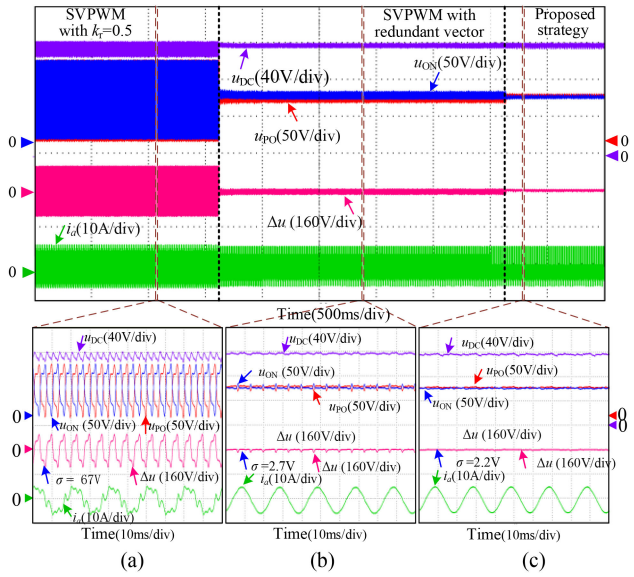

Fig. 15. Experimental results of different strategies when $m = 0.96$. (a) SVPWM strategy with $k_r = 0.5$. (b) SVPWM strategy with redundant vector modulation. (c) Proposed hybrid modulation strategy.

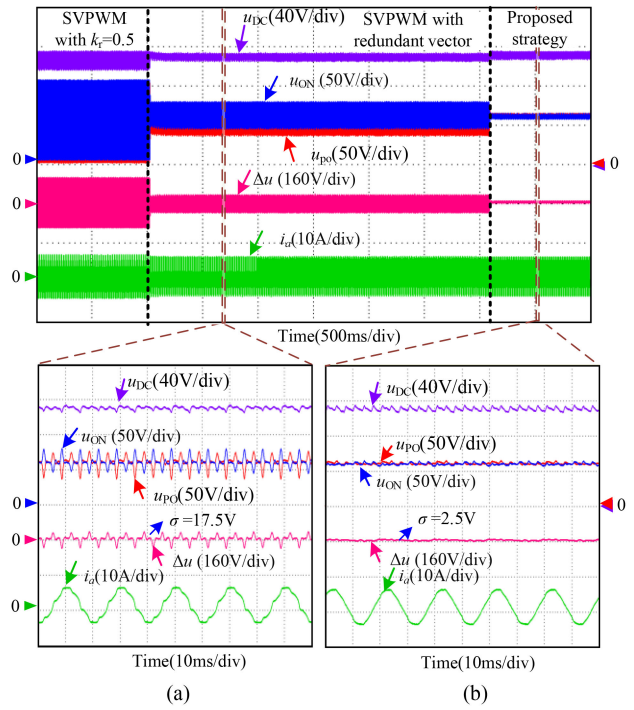

Fig. 16. Experimental results of different strategies when $m = 1$. (a) SVPWM strategy with redundant vector modulation. (b) Proposed hybrid modulation strategy.

NP balance due to the unbalanced intervals. In Fig. 15(c), the proposed strategy can basically eliminate the NP fluctuation and realize the NP balance, which proves the effectiveness of the proposed strategy. Experimental results of different strategies when $m = 1$ are shown in Fig. 16. It can be seen that the modulation of redundant vector cannot suppress the NP fluctuation, which causes higher voltage stress on dc-link capacitors and switching

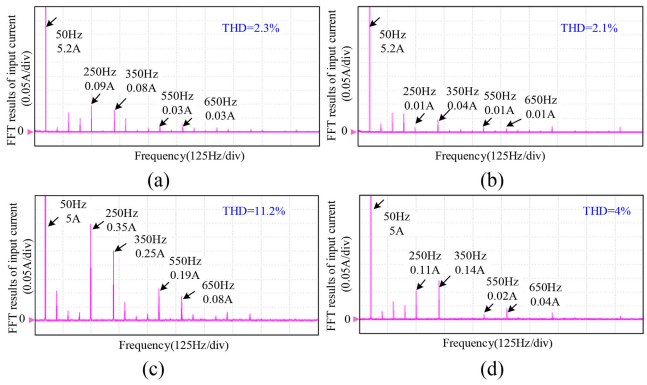

Fig. 17. FFT results under different m. (a) SVPWM under $m = 0.96$. (b) Proposed strategy under $m = 0.96$. (c) SVPWM under $m = 1$. (d) Proposed strategy under $m = 1$.

devices. In Fig. 16(b), the proposed strategy can also effectively suppress the NP fluctuation. The maximum RMS of Δu is 2.5 V, which is 16% of that of conventional SVWPM. Therefore, the proposed strategy can realize the NP balance and reduce the voltage stress.

The fast Fourier transform results under different m are shown in Fig. 17. It can be seen that the input currents mainly include the 5th, 7th, 11th, and 13th harmonics. Therefore, the NP fluctuation not only causes the voltage stress on dc-link capacitors, but also leads to the distortions of input currents. Comparing Fig. 17(a) and (c), it can be seen that the input current harmonics is proportional to m because of the increase of NP fluctuation. Comparing Fig. 17(b) and (d), the input current harmonics are also proportional to m because of the increase of phase error voltage. According to Fig. 17, it can be seen that the input current harmonics of the proposed strategy is lower than that of conventional SVPWM. Therefore, the proposed strategy can reduce harmonics of the input currents.

Fig. 18 shows experimental results of the proposed strategy under different τ. According to Fig. 18(a), the NP fluctuation and harmonics of input currents of $\tau = 1.06$ are the largest under $m = 0.97$. When $\tau = 1.02$, the NP fluctuation can be suppressed, which has slight oscillation. When $\tau = 1$, the NP fluctuation can be eliminated, but the total harmonic distortion (THD) of input currents increases slightly. According to Fig. 18(b), the NP fluctuation of $\tau = 1$ is the minimum when $m = 1$. The minimum THD of input currents is $\tau = 1.02$. Therefore, τ can change the NP fluctuation and THD of input currents. To reduce the NP fluctuation and harmonics of input currents, $\tau = 1.02$ is selected.

Fig. 19 shows dynamic operations of the proposed strategy. In Fig. 19(a), it can be seen that when the input phase voltage is 88% rated phase voltage, the NP fluctuation is nearly zero. When the input phase voltage is rated phase voltage, there is the slight NP fluctuation due to the increased m. As can be seen from Fig. 19(b), the NP fluctuation of $R = 60\ \Omega$ is lower than that of $R = 30\ \Omega$ due to the decrease of the input current, and the proposed strategy can remain stable when the dc-link load is abruptly changed. In Fig. 19, it can be seen that the maximum Δu and the THD of input currents are 3.5 V and

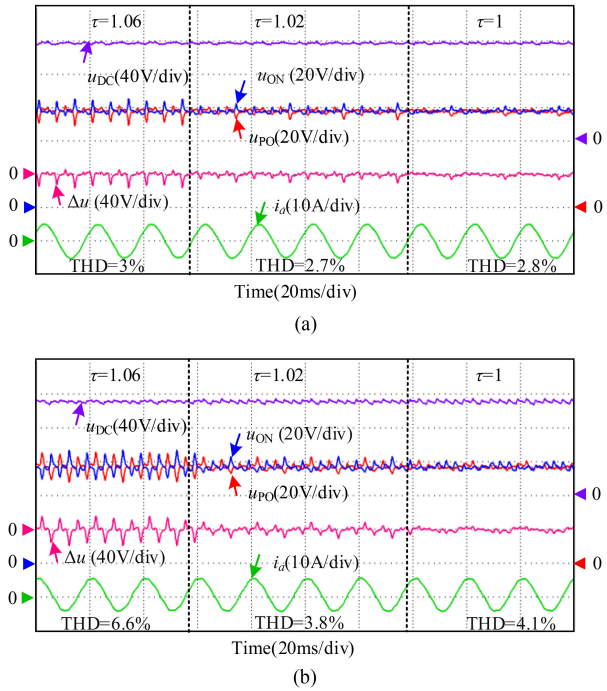

Fig. 18. Experimental results of the proposed strategy under different τ. (a) $m = 0.97$. (b) $m = 1$.

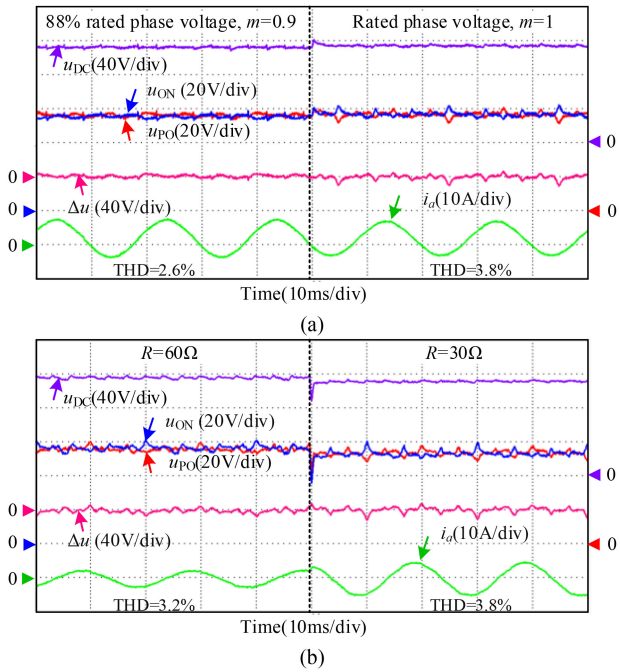

Fig. 19. Dynamic operations of the Vienna rectifier. (a) Input phase voltages are step-up from 88% rated phase voltage to rated phase voltage. (b) DC-link resistance is step-down from 60 to 30 Ω.

3.8%, respectively. Therefore, the proposed strategy can realize the NP voltage balance and input current harmonics reduction during dynamic operations of the Vienna rectifier.

Fig. 20 shows the experimental comparison results under different m. In Fig. 20(a), the NP fluctuation of the proposed strategy is proportional to m and τ. When $\tau = 1$, the maximum σ of the proposed strategy is 2.5 V, and the conventional

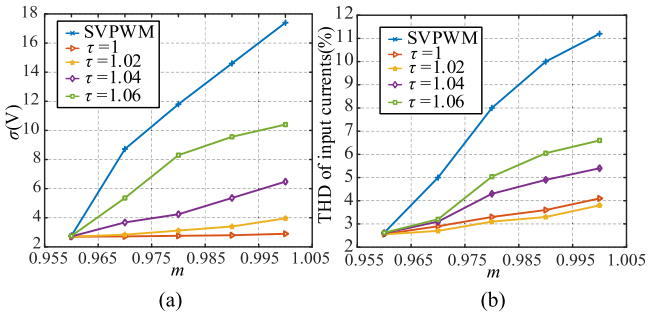

Fig. 20. Experimental comparison results under different m. (a) Experimental results of σ. (b) The experimental results of THD of input currents.

SVPWM is 17.5 V, which further verifies that the proposed strategy can realize the NP balance. According to Fig. 20(b), it can be seen that the THD of the proposed strategy is proportional to m. The THD of input currents of the proposed strategy is significantly lower than that of the conventional SVPWM. When $\tau = 1.02$, the THD of input currents is minimum, which is consistent with Fig. 11(b). Therefore, the phase voltage error can effectively analyze the input current harmonics of the proposed strategy. The execution times of the conventional SVPWM strategy and the proposed strategy are 5.6 and 5.8 μs, respectively. The execution time of the proposed strategy is slightly longer than that of the conventional SVPWM strategy, but it does not impose a burden on the system. Therefore, the proposed strategy has advantages in practical applications.

V Conclusion

In this article, a hybrid modulation strategy combining the modulations of redundant vector and compression vector is proposed. The NP-balance capability of conventional SVPWM for electrolytic capacitorless Vienna rectifiers is analyzed, and the NP fluctuation and the input current harmonics are larger with the largely reduced capacitors when modulation index is high. With the proposed strategy, the NP fluctuation of dc-link film capacitors can be suppressed by the compression coefficient. Additionally, by analyzing the model of phase voltage error, the input current harmonics can be reduced with the appropriate adjustment factor. The experimental results indicate that the proposed strategy has lower NP fluctuation and THD of input currents compared with conventional SVPWM.

References

[1] Y. Zou et al., "Dynamic-space-vector discontinuous PWM for three-phase Vienna rectifiers with unbalanced neutral-point voltage," *IEEE Trans. Power Electron.*, vol. 36, no. 8, pp. 9015–9026, Feb. 2021.

[2] J. Adhikari, P. Iv, and S. K. Panda, "Reduction of input current harmonic distortions and balancing of output voltages of the Vienna rectifier under supply voltage disturbances," *IEEE Trans. Power Electron.*, vol. 32, no. 7, pp. 5802–5812, Sep. 2017.

[3] T. Wang, C. Chen, P. Liu, T. Liu, Z. Chao, and S. Duan, "A hybrid space-vector modulation method for harmonics and current ripple reduction of interleaved vienna rectifier," *IEEE Trans. Ind. Electron.*, vol. 67, no. 10, pp. 8088–8099, Oct. 2020.

[4] T. Wang, C. Chen, P. Liu, W. Zhu, and S. Duan, "A current control method with extended bandwidth for Vienna rectifier considering wide inductance variation," *IEEE J. Emerg. Sel. Top. Power Electron.*, vol. 9, no. 1, pp. 590–601, Feb. 2021.
[5] W. Zhu, C. Chen, S. Duan, T. Wang, and P. Liu, "A carrier-based discontinuous PWM method with varying clamped area for Vienna rectifier," *IEEE Trans. Ind. Electron.*, vol. 66, no. 9, pp. 7177–7188, Sep. 2019.
[6] W. Ding, C. Zhang, F. Gao, B. Duan, and H. Qiu, "A zero-sequence component injection modulation method with compensation for current harmonic mitigation of a Vienna rectifier," *IEEE Trans. Power Electron.*, vol. 34, no. 1, pp. 801–814, Jan. 2019.
[7] R. Maheshwari, S. Munk-Nielsen, and S. Busquets-Monge, "Design of neutral-point voltage controller of a three-level NPC inverter with small dc-link capacitors," *IEEE Trans. Ind. Electron.*, vol. 60, no. 5, pp. 1861–1871, May 2013.
[8] Z. He et al., "A novel method to evaluate the influence of Vienna rectifier neutral-point voltage fluctuation on input current quality," *IEEE Trans. Power Electron.*, vol. 36, no. 7, pp. 8347–8358, Jul. 2021.
[9] J.-S. Lee and K.-B. Lee, "Performance analysis of carrier-based discontinuous PWM method for Vienna rectifiers with neutral-point voltage balance," *IEEE Trans. Power Electron.*, vol. 31, no. 6, pp. 4075–4084, Jun. 2016.
[10] P. Zhang, X. Wu, Z. Chen, W. Xu, J. Liu, and J. Qi, "A multizero-sequence component injection algorithm for a five-level flying capacitor rectifier under unbalanced dc-link voltages," *IEEE Trans. Power Electron.*, vol. 36, no. 10, pp. 11967–11983, Oct. 2021.
[11] W. Ding, H. Qiu, B. Duan, X. Xing, N. Cui, and C. Zhang, "A novel segmented component injection scheme to minimize the oscillation of dc-link voltage under balanced and unbalanced conditions for Vienna rectifier," *IEEE Trans. Power Electron.*, vol. 34, no. 10, pp. 9536–9551, Oct. 2019.
[12] L. J. Hang, B. Li, M. Zhang, Y. Wang, and L. M. Tolbert, "Equivalence of SVM and carrier-based PWM in three-phase/wire/level Vienna rectifier and capability of unbalanced-load control," *IEEE Trans. Ind. Electron.*, vol. 61, no. 1, pp. 20–28, Jan. 2014.
[13] S. B. Monge, S. Somavilla, J. Bordonau, and D. Boroyevich, "Capacitor voltage balance for the neutral-point- clamped converter using the virtual space vector concept with optimized spectral performance," *IEEE Trans. Power Electron.*, vol. 22, no. 4, pp. 1128–1135, Jul. 2007.
[14] S. Wang, N. Jiao, J. Ma, T. Liu, and X. Liu, "Analysis and optimization of voltage balancing control limits for cascaded h-bridge rectifiers," *IEEE Trans. Ind. Electron.*, vol. 68, no. 11, pp. 10677–10687, Nov. 2021.
[15] J.-S. Lee and K.-B. Lee, "A novel carrier-based PWM method for Vienna rectifier with a variable power factor," *IEEE Trans. Ind. Electron.*, vol. 63, no. 1, pp. 3–12, Jan. 2016.
[16] C.-Q. Xiang, C. Shu, D. Han, B.-K. Mao, X. Wu, and T.-J. Yu, "Improved virtual space vector modulation for three-level neutral-point-clamped converter with feedback of neutral-point voltage," *IEEE Trans. Power Electron.*, vol. 33, no. 6, pp. 5452–5464, Jun. 2018.
[17] J.-S. Lee, S. Yoo, and K.-B. Lee, "Novel discontinuous PWM method of a three-level inverter for neutral-point voltage ripple reduction," *IEEE Trans. Ind. Electron.*, vol. 63, no. 6, pp. 3344–3354, Jun. 2016.
[18] S. Wang, J. Ma, B. Liu, N. Jiao, T. Liu, and Y. Wang, "Unified SVPWM algorithm and optimization for single-phase three-level NPC converters," *IEEE Trans. Power Electron.*, vol. 35, no. 7, pp. 7702–7712, Jul. 2020.
[19] R. Burgos, R. X. Lai, Y. Q. Pei, F. Wang, D. Boroyevich, and J. Pou, "Space vector modulator for Vienna-type rectifiers based on the equivalence between two- and three-level converters: A carrier-based implementation," *IEEE Trans. Power Electron.*, vol. 23, no. 4, pp. 1888–1898, Jul. 2008.
[20] R. Lai, F. Wang, R. Burgos, D. Boroyevich, D. Jiang, and D. Zhang, "Average modeling and control design for Vienna-type rectifiers considering the dc-link voltage balance," *IEEE Trans. Power Electron.*, vol. 24, no. 11, pp. 2509–2522, Nov. 2009.
[21] W. Song et al., "A hybrid control method to suppress the three-time fundamental frequency neutral-point voltage fluctuation in a vienna rectifier," *IEEE J. Emerg. Sel. Top. Power Electron.*, vol. 4, no. 2, pp. 468–480, Jun. 2016.
[22] X. Li et al., "A generalized design framework for neutral point voltage balance of three-phase Vienna rectifiers," *IEEE Trans. Power Electron.*, vol. 34, no. 10, pp. 10221–10232, Oct. 2019.
[23] D. A. Molligoda et al., "Hybrid modulation strategy for the Vienna rectifier," *IEEE Trans. Power Electron.*, vol. 37, no. 2, pp. 1283–1295, Feb. 2022.
[24] X. Xing, X. Li, C. Qin, Z. Liu, and C. Zhang, "Two-layer pulsewidth modulation strategy for common-mode voltage and current harmonic distortion reduction in Vienna rectifier," *IEEE Trans. Ind. Electron.*, vol. 67, no. 9, pp. 7470–7483, Sep. 2020.
[25] J.-S. Lee and K.-B. Lee, "Carrier-based discontinuous PWM method for Vienna rectifiers," *IEEE Trans. Power Electron.*, vol. 30, no. 6, pp. 2896–2900, Jun. 2015.
[26] M. M. Hashempour, M. Yang, and T. Lee, "An adaptive control of DPWM for clamped-three-level photovoltaic inverters with unbalanced neutral-point voltage," *IEEE Trans. Ind. Appl.*, vol. 54, no. 6, pp. 6133–6148, Nov./Dec. 2018.
[27] Z. He et al., "A hybrid DPWM for Vienna rectifiers based on the three-level to two-level conversion," *IEEE Trans. Ind. Electron.*, vol. 69, no. 9, pp. 9429–9439, Sep. 2022.
[28] L. Zhang et al., "A modified DPWM with neutral point voltage balance capability for three-phase Vienna rectifiers," *IEEE Trans. Power Electron.*, vol. 36, no. 1, pp. 263–273, Jan. 2021.
[29] N. Celanovic and D. Boroyevich, "A comprehensive study of neutral-point voltage balancing problem in three-level neutral-point-clamped voltage source PWM inverters," *IEEE Trans. Power Electron.*, vol. 15, no. 2, pp. 242–249, Mar. 2000.
[30] X. Wu, G. Tan, Z. Ye, G. Yao, Z. Liu, and G. Liu, "Virtual-space-vector PWM for a three-level neutral-point-clamped inverter with unbalanced dc-links," *IEEE Trans. Power Electron.*, vol. 33, no. 3, pp. 2630–2642, Mar. 2018.
[31] S. Busquets-Monge, J. Bordonau, D. Boroyevich, and S. Somavilla, "The nearest three virtual space vector PWM - a modulation for the comprehensive neutral-point balancing in the three-level NPC inverter," *IEEE Power Electron. Lett.*, vol. 2, no. 1, pp. 11–15, Mar. 2004.
[32] J. Pou et al., "Fast-processing modulation strategy for the neutral-point-clamped converter with total elimination of low-frequency voltage oscillations in the neutral point," *IEEE Trans. Ind. Electron.*, vol. 54, no. 4, pp. 2288–2294, Aug. 2007.
[33] A. K. Gupta and A. M. Khambadkone, "A simple space vector PWM scheme to operate a three-level NPC inverter at high modulation index including overmodulation region, with neutral point balancing," *IEEE Trans. Ind. Appl.*, vol. 43, no. 3, pp. 751–760, May/Jun. 2007.

Zhijian Zhang received the B.S. degree in electrical engineering from the North University of China, Taiyuan, China, in 2018, and the M.S. degree in electrical engineering from Beijing Jiaotong University, Beijing, China, in 2021. He is currently working toward the Ph.D. degree in power electronics and electrical drives with the Harbin Institute of Technology, Harbin, China.

His current research interests include permanent magnet synchronous motor control, high efficiency ac–dc converter, and Vienna rectifier control.

Guoqiang Zhang (Senior Member, IEEE) received the B.S. degree in electrical engineering from Harbin Engineering University, Harbin, China, in 2011, and the M.S. and Ph.D. degrees in electrical engineering from the Harbin Institute of Technology, Harbin, China, in 2013 and 2017, respectively.

Since 2017, he has been in the Department of Electrical Engineering, Harbin Institute of Technology, where he is currently an Associate Professor. His current research interests include control of electrical drives, and parameter identification technique, with main focus on sensorless field-oriented control of synchronous motor drives.

Dr. Zhang serves as an Associate Editor for the *Journal of Power* Electronics.

Gaolin Wang (Senior Member, IEEE) received the B.S., M.S. and Ph.D. degrees in electrical engineering from Harbin Institute of Technology, Harbin, China, in 2002, 2004 and 2008 respectively.

In 2009, he joined the Department of Electrical Engineering, Harbin Institute of Technology as a Lecturer, where he has been a Full Professor of Electrical Engineering since 2014. From 2009 to 2012, he was a Postdoctoral Fellow in Shanghai Step Electric Corporation, where he was involved in the traction machine control for direct-drive elevators. He has authored more than 60 technical papers published in IEEE Transactions. He is the holder of 30 Chinese patents. His current major research interests include permanent magnet synchronous motor drives, position sensorless control of AC motors, and digital control of power converters.

Dr. Wang serves as a Guest Associate Editor of IEEE TRANSACTIONS ON INDUSTRIAL ELECTRONICS, an Associate Editor of IEEE TRANSACTIONS ON TRANSPORTATION ELECTRIFICATION, *IET Electric Power Applications*, and *Journal of Power Electronics*.

Jiarui Wang received the B.S. degree in electrical engineering in 2021 from the Harbin Institute of Technology, Harbin, China, where he is currently working toward the M.S. degree in power electronics and electrical drives.

His current research interests include control of Vienna rectifier and high efficiency ac–dc converter.

Dawei Ding (Member, IEEE) received the B.S. and M.S. degrees in electrical engineering from Hefei University of Technology, Hefei, China, in 2014 and 2017, respectively, and the Ph.D. degree in electrical engineering from Harbin Institute of Technology (HIT), Harbin, China, in 2021.

He is currently an Assistant Professor with the School of Electrical Engineering and Automation, HIT. From 2020 to 2021, he was a visiting Ph.D. with Technical University of Denmark. He has authored more than 10 journal papers in IEEE Transactions. His current research interests include advanced control of permanent magnet synchronous motor drives and electrolytic capacitorless ac motor drives.

Dianguo Xu (Fellow, IEEE) received the B.S. degree in control engineering from Harbin Engineering University, Harbin, China, in 1982, and the M.S. and Ph.D. degrees in electrical engineering from Harbin Institute of Technology (HIT), Harbin, in 1984 and 1989, respectively.

In 1984, he was an Assistant Professor with the Department of Electrical Engineering, HIT. Since 1994, he has been a Professor with the Department of Electrical Engineering, HIT. He was the Dean of School of Electrical Engineering and Automation, HIT, from 2000 to 2010. He is currently the Vice President of HIT. He has authored or coauthored more than 600 technical papers. His research interests include renewable energy generation technology, power quality mitigation, sensorless vector controlled motor drives, and high performance servo system.

Dr. Xu is currently an Associate Editor for IEEE TRANSACTIONS ON INDUSTRIAL ELECTRONICS and IEEE JOURNAL OF EMERGING AND SELECTED TOPICS IN POWER ELECTRONICS. He is currently the Chairman of IEEE Harbin Section.